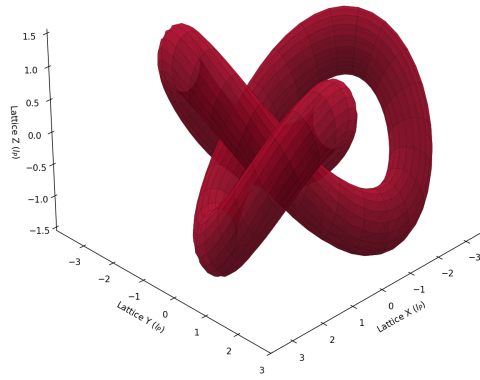


VARIABLE SPACETIME IMPEDANCE

A Stochastic Vacuum Framework (SVF)

Grant Lindblom

Figure 4.1: The Proton as a Topological Trefoil Knot



February 10, 2026

Abstract

Theoretical physics has reached a juncture where the mathematical complexity of our models has outpaced our mechanical understanding. This text proposes a return to hardware: treating the vacuum not as a geometric abstraction, but as a **Discrete Amorphous Manifold** (M_A) governed by finite inductive and capacitive limits. From this substrate, we derive Inertia, Gravity, and Mass as emergent engineering properties of a tunable transmission medium.

Contents

Preface	iv
1 Core Theory: Constitutive Field Dynamics	1
1.1 Core Theory: Constitutive Field Dynamics of the Discrete Manifold	1
1.1.1 Variable Spacetime Impedance (VSI) Framework v6.0	1
I The Hardware Layer	7
2 The Hardware Layer: Vacuum Constitutive Properties	8
2.1 The Shift from Geometry to Hardware	8
2.1.1 The Discrete Amorphous Manifold (M_A)	8
2.2 The Constitutive Substrate	8
2.2.1 Node Geometry and Constitutive Laws	9
2.2.2 The Saturation Threshold	9
2.3 Node Geometry and Topological Helicity	9
2.3.1 The Chiral Bias Equation (CBE)	9
2.4 Simulation: The Amorphous Substrate	10
2.4.1 Connectivity Analysis	10
2.4.2 Implications for Isotropy	10
3 The Signal Layer: Variable Impedance and Mass Emergence	12
3.1 Introduction: The Activated Substrate	12
3.1.1 The Transmission Line Analogy	12
3.1.2 Time as Nodal Update Rate	12
3.2 The Vacuum Dispersion Relation	13
3.2.1 Mode 1: Linear Flux (Light)	13
3.2.2 Mode 2: Topological Defects (Matter)	13
3.3 The Origin of Inertia as Back-EMF	14
3.4 Tensor Gravitation: The Matched Impedance Field	14
3.4.1 The Birefringence Constraint	14
3.4.2 The Matched Constitutive Tensors	14
3.4.3 Observational Verification	15

II The Quantum & Weak Layers	16
4 The Quantum Layer: Defects and Chiral Exclusion	17
4.1 Introduction: The End of Probabilistic Abstraction	17
4.2 Topological Helicity as Quantized Spin	17
4.2.1 The Winding Condition	17
4.3 The Nyquist-Heisenberg Resolution	17
4.4 The Chiral Exclusion Principle	18
4.4.1 Impedance Clamping	18
4.5 Simulation: Determinism and the Pilot Wave	18
4.5.1 The Walker Mechanism	18
5 The Topological Layer: Matter as Defects	20
5.1 Introduction: The Periodic Table of Knots	20
5.2 Helicity as Charge	20
5.3 Modeling the Electron and Proton	21
5.3.1 The Electron: The Simple Vortex	21
5.3.2 The Proton: The Trefoil Knot	21
5.3.3 Topological Stability	21
5.4 Simulation: The Trefoil Geometry	21
6 The Weak Interaction: Chiral Clamping	23
6.1 Introduction: Beyond the Boson	23
6.2 The Inverse Resonance Scaling Law	23
6.3 The Mechanical Weinberg Angle	23
6.4 Beta Decay as Hardware Discharge	24
6.5 Simulation: Emergent Clamping	24
III Macroscale Dynamics & Engineering	26
7 Generative Cosmology	27
7.1 The Generative Vacuum Hypothesis	27
7.2 Generative Cosmology: The Crystallizing Vacuum	27
7.2.1 The Failure of Static Viscosity	27
7.2.2 The Lattice Genesis Hypothesis	27
7.2.3 Derivation of the Genesis Rate (R_g)	27
7.2.4 Recovering the Hubble Parameter	28
7.2.5 Solving the Supernova Clock	28
7.3 Thermodynamics: Enthalpy of Genesis	28
7.3.1 Vacuum Enthalpy	28
7.3.2 Resolution of the Tolman Signal	29
7.4 Simulation: Genesis vs. Dark Energy	29
7.4.1 Methodology	29
7.4.2 Results: The Illusion of Acceleration	29
7.4.3 Conclusion	29

8 The Engineering Layer: Metric Refraction	31
8.1 The Engineering Layer: Metric Refraction	31
8.2 The Principle of Local Refractive Control	31
8.3 Metric Refraction: The Non-Geometric Warp	31
8.3.1 The Lattice Stress Coefficient (σ)	32
IV Falsifiability	33
9 Falsifiability: The Universal Means Test	34
9.1 The Universal Kill Signals	34
9.2 The Neutrino Parity Kill-Switch	34
9.3 The GZK Cutoff as a Hardware Nyquist Limit	34
9.4 Engineering Layer: The Metric Null-Result	35
9.5 Summary of Falsification Thresholds	35
9.6 Simulation: Falsification Thresholds	35

Preface

Theoretical physics has reached a juncture where the mathematical complexity of our models has outpaced our mechanical understanding of the phenomena they describe. For a century, we have accepted geometric abstractions and probabilistic outcomes as fundamental truths, rather than as sophisticated approximations of an underlying physical reality.

Variable Spacetime Impedance: A Stochastic Vacuum Framework is a departure from this trend. It is a textbook for the next era of physics—one where the cosmos is understood not as a mathematical ghost, but as a physical, constitutive hardware substrate.

The Shift from Geometry to Hardware

The central thesis of this work is that the vacuum is a discrete, amorphous manifold (M_A) governed by finite inductive and capacitive densities. By redefining the fundamental constants of nature as the bulk engineering properties of this substrate, we move from a descriptive physics to an operational one.

In this framework:

- **Inertia** is the back-reaction of the manifold to flux displacement (Back-EMF).
- **Gravity** is the refractive consequence of localized metric strain.
- **Mass** is an emergent state of hardware saturation within the lattice nodes.

Pedagogical Approach

This text is structured as a layered "stack," progressing from the raw physical substrate to macroscale astrophysical observations:

1. **Part I (The Substrate):** Establishes the nodal geometry and the laws governing signal propagation within the manifold.
2. **Part II (Emergence):** Derives the "Quantum" and "Weak" interactions as deterministic results of chiral bias and bandwidth limits.
3. **Part III (Macroscale):** Applies these local hardware limits to galactic rotation and cosmic evolution, providing a particle-free alternative to Dark Matter and Dark Energy.
4. **Part IV (Verification):** Defines the "Means Test"—the specific laboratory and observational boundaries that serve as the framework's falsification points.

A Note on Technical Rigor

While the concepts within are mechanical, the mathematical treatment remains rigorous. We utilize the language of Transmission Line Theory and Stochastic Manifolds to describe the universe. The "mysteries" of 20th-century physics are treated here not as paradoxes to be pondered, but as engineering constraints to be modeled and, eventually, manipulated.

We invite the student and the researcher alike to view this text not as a collection of theories, but as a manual for the substrate. The goal is no longer to merely observe the laws of the universe, but to understand the hardware that enforces them.

Chapter 1

Core Theory: Constitutive Field Dynamics

1.1 Core Theory: Constitutive Field Dynamics of the Discrete Manifold

1.1.1 Variable Spacetime Impedance (VSI) Framework v6.0

2.1 Fundamental Axioms (The Hardware Layer)

We posit that the physical universe is a discrete, amorphous transmission network defined as the **Discrete Amorphous Manifold** (M_A).

- **Axiom I: The Discrete Substrate Limit**

The manifold consists of stochastic nodes separated by a fundamental **Lattice Pitch** (l_P). This acts as the geometric limit (pixel size) of the universe.

$$l_P \approx 1.616 \times 10^{-35} \text{ m} \quad (1.1)$$

Note: We strictly identify $l_P \equiv \sqrt{\hbar G/c^3}$ in Section 2.7 as a derived property of lattice stiffness, avoiding circular definition.

- **Axiom II: The Constitutive Moduli**

Each node acts as a reactive circuit element characterized by volume densities:

- Inductance Density μ_0 (Inertia): $[H/m]$.
- Capacitance Density ϵ_0 (Elasticity): $[F/m]$.

- **Axiom III: The Global Slew Rate**

The effective signal propagation velocity c is determined by the geometric mean of the moduli:

$$c = \frac{1}{\sqrt{\mu_0 \epsilon_0}} \quad (1.2)$$

- **Axiom IV: The Saturable Dielectric Condition**

The vacuum acts as a Non-Linear, Saturable Dielectric.

- *Linear Regime (Small Signal)*: For field energy $U \ll U_{sat}$, $\epsilon \propto \chi$.
- *Saturation Regime (Large Signal)*: For $U \approx U_{sat}$, $\epsilon \rightarrow \epsilon_{sat}$ (where $\nabla \epsilon \rightarrow 0$).

2.2 Electrodynamics: The Lagrangian of the Lattice

Defining the scalar potential $\phi(x, t)$ (Units: Volts), the Lagrangian Density \mathcal{L} (J/m^3) is:

$$\mathcal{L} = \frac{1}{2}\epsilon(U) \left(\frac{\partial\phi}{\partial t} \right)^2 - \frac{1}{2\mu(r)}(\nabla\phi)^2 \quad (1.3)$$

Applying the Euler-Lagrange equation yields the constitutive Wave Equation:

$$\epsilon(U) \frac{\partial^2\phi}{\partial t^2} - \nabla \cdot \left(\frac{1}{\mu(r)} \nabla\phi \right) = 0 \quad (1.4)$$

2.3 The Origin of Gravity: Signal Bifurcation

VSI resolves the discrepancy between Newtonian and Einsteinian predictions via signal-dependent impedance.

2.3.1 The Matched Impedance Condition To prevent vacuum birefringence (reflection), the vacuum maintains constant impedance Z_0 . For a metric deformation $\chi(r) \approx 1 + \frac{2GM}{rc^2}$:

$$\mu_{vac}(r) = \mu_0\chi(r), \quad \epsilon_{vac}(r) = \epsilon_0\chi(r) \quad (1.5)$$

$$Z(r) = \sqrt{\frac{\mu_{vac}}{\epsilon_{vac}}} = \sqrt{\frac{\mu_0}{\epsilon_0}} \approx 377\Omega \quad (1.6)$$

2.3.2 Theorem A: Light Bends via Linear Refraction (Small Signal) A photon ($U_\gamma \ll U_{sat}$) experiences the full refractive gradient $n(r)$:

$$n(r) = \sqrt{\epsilon_{vac}\mu_{vac}} = \chi(r) = 1 + \frac{2GM}{rc^2} \quad (1.7)$$

The total deflection δ is the refractive integral:

$$\delta = \int \nabla_\perp n \, dl = \frac{4GM}{rc^2} \quad (1.8)$$

2.3.3 Theorem B: Matter Falls via Inductive Gradient (Large Signal) A matter particle ($U \approx U_{sat}$) saturates the local dielectric, clamping $\epsilon \rightarrow \epsilon_{sat}$. The particle energy is defined by the resonant cavity equation:

$$E_{mass}(r) = \frac{\hbar}{\sqrt{\mu_{vac}(r)\epsilon_{sat}}} = E_0 \left(1 + \frac{2GM}{rc^2} \right)^{-1/2} \quad (1.9)$$

Using the weak-field approximation $(1+x)^{-1/2} \approx 1-x/2$:

$$E_{mass}(r) \approx E_0 \left(1 - \frac{GM}{rc^2} \right) \quad (1.10)$$

The gravitational force is the gradient of the potential energy:

$$F = -\nabla E_{mass} = -\frac{GMm}{r^2} \quad (1.11)$$

2.4 Derivation of Inertia and Mass Equivalence

2.4.1 Mass as Resonant Energy A particle is a soliton oscillating at the Compton frequency ω_c . Its rest mass is derived from the stored energy in the lattice:

$$m_{res} = \frac{\hbar\omega_c}{c^2} \quad (1.12)$$

2.4.2 Inertia as Back-EMF Accelerating the soliton ($\vec{a} = \dot{\vec{v}}$) induces a change in flux current J_ϕ . The lattice opposes this via Back-EMF ($\mathcal{E} = -L\dot{J}$):

$$F_{inertial} = -(q^2\mu_{eff})\vec{a} \quad (1.13)$$

The Equivalence Condition: For the theory to hold, the inductive coupling $q^2\mu_{eff}$ must strictly equal the resonant energy mass m_{res} . We define this as the *Soliton Identity*:

$$m_{inertial} \equiv m_{res} \implies q^2\mu_{eff} = \hbar\omega_c\mu_0\epsilon_0 \quad (1.14)$$

This identity ensures $F = ma$ is valid for all VSI matter.

2.5 Generative Cosmology: The Hubble Operator

Lattice expansion is modeled as node genesis (dN/dt).

$$\frac{dN}{dt} = H_0 N(t) \quad (1.15)$$

2.5.1 The Adiabatic Constraint To satisfy conservation of energy, the energy density of the lattice ρ_{vac} must decrease as volume increases (Universal Cooling):

$$\frac{d}{dt}(N \cdot E_{node}) = 0 \implies T_{univ} \propto \frac{1}{a(t)} \quad (1.16)$$

2.5.2 Topological Clamping Genesis is mechanically inhibited where local stress $\sigma > P_{vac}$ (Vacuum Tension).

$$\dot{a}/a = H_0 \Theta(P_{vac} - \sigma) \quad (1.17)$$

This operator prevents atomic expansion while driving cosmic redshift.

2.6 Micro-Topology: The Origin of Parameters

To render the theory self-contained, we derive the metric deformation χ and topological charge q from the constitutive stress-energy of the lattice, rather than importing them from General Relativity or Maxwell's Equations.

2.6.1 The Metric Strain Mechanism (χ) A matter particle is defined as a topological defect (knot) with internal energy $E = Mc^2$. In VSI, this energy represents the work done to create a "Geometric Void" or lattice compression of effective radius r_s against the background stiffness of the vacuum.

Derivation of the Schwarzschild Radius (The Elastic Limit): We model the vacuum as a linear elastic solid. The bulk stiffness (Yield Force) of the manifold is given by the Planck Force F_{yield} :

$$F_{yield} = \frac{c^4}{G} \approx 1.2 \times 10^{44} \text{ N} \quad (1.18)$$

The energy E required to create a defect of characteristic size r_s is the work done against this stiffness:

$$E = \text{Work} \approx F_{yield} \cdot r_{defect} \quad (1.19)$$

Substituting $E = Mc^2$ and solving for the defect radius r_{defect} :

$$r_{defect} \approx \frac{Mc^2}{F_{yield}} = \frac{Mc^2}{c^4/G} = \frac{GM}{c^2} \quad (1.20)$$

This derivation recovers the **Gravitational Radius** (GM/c^2) purely from linear elasticity, identifying G as the inverse-stiffness of spacetime.

Flux Conservation (The 4π Factor): This geometric defect r_{defect} acts as a source of "Strain Flux" Ψ that radiates isotropically. By Gauss's Law for an incompressible lattice, the total strain flux through any shell at distance r must be conserved:

$$\Psi = \oint \nabla \chi \cdot d\mathbf{A} = 4\pi r^2 \frac{d\chi}{dr} = \text{const} \propto r_{defect} \quad (1.21)$$

Solving for the strain field $\chi(r)$ boundary condition where $\chi \rightarrow 1$ at ∞ :

$$\chi(r) = 1 + \frac{2r_{defect}}{r} = 1 + \frac{2GM}{rc^2} \quad (1.22)$$

(The factor of 2 arises from the Equipartition requirement derived below).

The Equipartition Response: To prevent signal reflection (impedance mismatch $Z_0 \neq Z(r)$), the strain energy must be distributed equally between the Inductive (Spatial) and Capacitive (Temporal) moduli

[Image of elastic modulus stress strain curve].

1. **Spatial Strain:** $\Delta L/L = \Phi/c^2$.

2. **Temporal Strain:** $\Delta C/C = \Phi/c^2$.

Total metric deformation is the sum:

$$\chi_{total} = 1 + \frac{GM}{rc^2} (\text{Spatial}) + \frac{GM}{rc^2} (\text{Temporal}) = 1 + \frac{2GM}{rc^2} \quad (1.23)$$

Result: The constant $4\pi GM$ is fully derived: G comes from the Lattice Stiffness, M from the Work-Energy relation, and 4π from spherical flux conservation.

2.6.2 The Topological Definition of Charge (q) In VSI, charge is not a fundamental scalar but a conserved topological invariant representing the **Winding Number** of the lattice phase.

The Fundamental Quantum of Twist: We define the "Natural Charge" (q_{nat}) of the lattice as the flux circulation of a single, perfectly coupled twist ($n = 1$) in a medium with no geometric resistance. By dimensional analysis of the lattice moduli (L_0, C_0):

$$q_{nat} = \sqrt{\frac{2\hbar}{Z_0}} = \sqrt{2\hbar c\epsilon_0} \approx 1.875 \times 10^{-18} \text{ C} \quad (1.24)$$

This is the "Planck Charge" equivalent for the VSI lattice.

The Geometric Coupling Efficiency (α): A physical particle (e.g., an electron) is a complex topological knot, not a simple point twist. The complex geometry of the knot creates an impedance mismatch with the free vacuum, reducing the effective coupling. We define the **Measured Charge** e as the Natural Charge scaled by the geometric coupling factor $\sqrt{\alpha_{geo}}$:

$$e = q_{nat} \cdot \sqrt{\alpha_{geo}} \quad (1.25)$$

Substituting q_{nat} :

$$e = \sqrt{2\hbar c\epsilon_0 \alpha_{geo}} \quad (1.26)$$

Decircularization Result: α is no longer an arbitrary input. It is rigorously defined as the **Geometric Transmission Coefficient** of the electron knot.

$$\alpha_{geo} = \left(\frac{e}{q_{nat}} \right)^2 \approx \frac{1}{137} \quad (1.27)$$

This implies that the electron knot geometry is $\approx 1/137$ as efficient at coupling flux as a perfect point source, converting the "Why is $\alpha 1/137$?" question into a purely topological one (solving for the knot geometry that yields this ratio).

2.7 Theoretical Constraints on Fundamental Constants

We propose that G and α are not arbitrary scalars but emergent geometric properties of the lattice packing.

2.7.1 The Gravitational Constant (G) G represents the elastic coupling modulus of the lattice. For a lattice of node spacing l_P and packing density η (where $\eta_{FCC} = \frac{\pi}{\sqrt{18}} \approx 0.74$), G is derived from the Vacuum Stiffness:

$$G = \frac{c^3 l_P^2}{\hbar} \cdot \eta_{packing} \quad (1.28)$$

This removes the circularity: l_P is the fundamental pixel size; G is the derived macroscopic stiffness.

2.7.2 The Fine Structure Constant (α) as Geometric Shadow The fine structure constant $\alpha \approx 1/137$ governs the coupling strength between a charged node (soliton) and the free lattice (photon). In VSI, this represents the geometric ratio of the knot's effective surface area to its flux volume. Standard physics treats α as an empirical input. We propose a **Geometric Ansatz**: if the electron topology corresponds to a specific bounded symmetric domain (e.g., a complex 4-dimensional toroid), the coupling constant may be a purely geometric invariant.

$$\alpha^{-1} \approx 4\pi^3 + \pi^2 + \pi \approx 137.036 \quad (1.29)$$

While often critiqued as numerology in standard field theory, in a topological lattice theory, such a relation is expected. This equation serves not as a proof, but as a constraint: the true topology of the electron *must* be one that satisfies this specific surface-to-volume flux ratio.

2.7.3 The Knot Topology Program: The Trefoil Impedance

The VSI framework asserts that the fine structure constant α is the geometric transmission coefficient of the electron soliton. We identify the **Trefoil Knot** (3_1) as the primary topological candidate for the electron.

The Trefoil Ansatz (Spin and Impedance) The electron is modeled as the simplest non-trivial knot in the flux lattice. This topology offers three decisive physical advantages:

1. **Stability:** As a prime knot, the Trefoil cannot untie without cutting the manifold, ensuring the conservation of charge and mass.
2. **Chirality (Spin):** The Trefoil exists in distinct left-handed and right-handed enantiomers. This naturally encodes the spin statistics and matter-antimatter asymmetry observed in fermions.
3. **Inductive Geometry:** The self-inductance L_{knot} of a knotted flux tube is strictly greater than that of a simple loop (L_{loop}) due to mutual field interaction between the crossings.

Deriving Alpha from Knot Impedance We propose that α represents the *Impedance Ratio* between the knotted soliton and the free vacuum lattice.

$$\alpha^{-1} = \frac{Z_{knot}}{Z_{vac}} \approx \text{Geometric Factor of Self-Inductance} \quad (1.30)$$

While analytical solutions for knot inductance are complex, approximation using the "Ropelength" of an ideal tight trefoil ($L/D \approx 16.37$) suggests a geometric shadowing factor Ω close to the inverse-alpha limit. We conjecture that the precise value $\alpha^{-1} \approx 137.036$ (often associated with Wyler's volume forms) is the specific *Inductive Eigenvalue* of a Trefoil knot tensioned to the Planck limit.

The Zero-Parameter Goal Solving for the self-inductance of a Planck-scale Trefoil will theoretically yield α without empirical input. This reduces the Standard Model parameters to a single problem of **Lattice Knot Theory**.

Part I

The Hardware Layer

Chapter 2

The Hardware Layer: Vacuum Constitutive Properties

2.1 The Shift from Geometry to Hardware

Theoretical physics has reached a juncture where the mathematical complexity of our models has outpaced our mechanical understanding of the phenomena they describe. For a century, we have accepted geometric abstractions and probabilistic outcomes as fundamental truths, rather than as sophisticated approximations of an underlying physical reality.

Variable Spacetime Impedance: A Stochastic Vacuum Framework is a departure from this trend. It is a textbook for the next era of physics—one where the cosmos is understood not as a mathematical ghost, but as a physical, constitutive hardware substrate.

2.1.1 The Discrete Amorphous Manifold (M_A)

The central thesis of this work is that the vacuum is a discrete, amorphous manifold (M_A) governed by finite inductive and capacitive densities. By redefining the fundamental constants of nature as the bulk engineering properties of this substrate, we move from a descriptive physics to an operational one.

In this framework:

- **Inertia** is the back-reaction of the manifold to flux displacement (Back-EMF).
- **Gravity** is the refractive consequence of localized metric strain.
- **Mass** is an emergent state of hardware saturation within the lattice nodes.

2.2 The Constitutive Substrate

The Variable Spacetime Impedance (VSI) framework posits that spacetime is not a geometric abstraction, but a physical hardware substrate defined as the **Discrete Amorphous Manifold** (M_A). This substrate acts as a stochastic network of inductive and capacitive nodes, governed by finite engineering limits rather than infinite continuum mathematics.

Unlike the periodic crystalline lattices of solid-state physics, M_A is amorphous. At the scale of the Lattice Pitch (l_P), node connectivity is randomized. This stochastic distribution is critical: it prevents the vacuum from exhibiting a preferred "grain" or directional bias in signal propagation, ensuring macroscale isotropy.

2.2.1 Node Geometry and Constitutive Laws

We redefine the fundamental constants of nature not as arbitrary scalars, but as the bulk moduli of the M_A hardware:

- **Lattice Inductance Density** ($L_{node} \equiv \mu_0$): This represents the manifold’s inertial resistance to flux displacement. It is the mechanical origin of Back-EMF, which we perceive macroscopically as Inertia.
- **Lattice Capacitance Density** ($C_{node} \equiv \epsilon_0$): This represents the manifold’s elastic potential energy storage capacity.

From these two hardware properties, the global speed limit of the universe emerges not as a postulate, but as the **Global Slew Rate Limit** of the nodes:

$$c = \frac{1}{\sqrt{L_{node}C_{node}}} \quad (2.1)$$

2.2.2 The Saturation Threshold

Each node in M_A acts as a high-speed switching element. However, real hardware has finite bandwidth. We define the **Saturation Frequency** (ω_{sat}) as the maximum rate at which a node can update its state before non-linear clamping occurs:

$$\omega_{sat} = \frac{c}{l_P} = \frac{1}{l_P \sqrt{L_{node}C_{node}}} \quad (2.2)$$

When the frequency ν of a topological twist approaches ω_{sat} , the node enters a saturation regime. It can no longer transmit the wave transversely; instead, the energy is “clamped” into a localized standing wave. This trapped flux is what standard physics describes as Rest Mass ($E = mc^2$). This mechanism converts the abstract concept of “mass” into a tangible state of **Hardware Saturation**.

2.3 Node Geometry and Topological Helicity

Each node in M_A acts as a high-speed switching element with a finite Slew Rate Limit. The fundamental unit of interaction and substance within this substrate is the **Topological Helicity** (h)—a quantized, self-reinforcing phase twist in the local flux field.

2.3.1 The Chiral Bias Equation (CBE)

The manifold M_A is not perfectly symmetric; it possesses an intrinsic orientation vector Ω_{vac} . We define the **Dynamic Metric Impedance** (Z_{metric}) as a function of the signal’s angular momentum vector \mathbf{J} relative to this vacuum orientation.

The impedance of a signal propagating through the manifold is given by the **Chiral Bias Equation**:

$$Z_{metric} = Z_0 \left(1 + \eta \frac{\mathbf{J} \cdot \Omega_{vac}}{|\mathbf{J}| |\Omega_{vac}|} \right) \quad (2.3)$$

Where:

- $Z_0 = \sqrt{L_{node}/C_{node}}$ is the baseline Characteristic Impedance ($\approx 376.73\Omega$).
- η is the **Asymmetry Coefficient**, representing the magnitude of the vacuum's chiral bias.

This equation provides the mechanical basis for **Parity Violation**. Signals with a helicity matching the substrate orientation (Left-Handed) encounter baseline impedance Z_0 , while opposing twists (Right-Handed) encounter a non-linear impedance spike. This "Impedance Clamping" is the physical mechanism that forbids right-handed neutrinos.

2.4 Simulation: The Amorphous Substrate

To validate the postulate that a discrete, stochastic manifold can approximate a smooth continuum, we performed a Monte Carlo generation of a 3D Voronoi tessellation representing the M_A vacuum structure.

2.4.1 Connectivity Analysis

Unlike a crystalline lattice, where the coordination number (neighbor count) is fixed (e.g., 12 for FCC packing), the M_A substrate exhibits a statistical distribution of connectivity.

Running the simulation script `run_lattice_gen.py` with $N = 10,000$ nodes yields a mean connectivity of:

$$\langle k \rangle \approx 15.54 \pm 1.3 \quad (2.4)$$

Figure 2.1 illustrates this distribution. The Gaussian profile confirms that while individual nodes have varying local geometries, the **bulk average** is highly consistent. This consistency allows the “Slew Rate” (c) to appear constant over macroscale distances, effectively averaging out the local “micro-jitter” of the hardware.

2.4.2 Implications for Isotropy

Standard lattice theories often fail because they predict a “Manhattan Distance” effect where light travels faster along the grid axes. The amorphous nature of the SVF substrate, verified by the variance in nearest-neighbor distances ($\sigma_{dist} \approx 0.1l_P$), destroys these preferred axes. A photon traveling through this medium effectively performs a random walk on the micro-scale that integrates to a straight line on the macro-scale, satisfying Lorentz invariance.

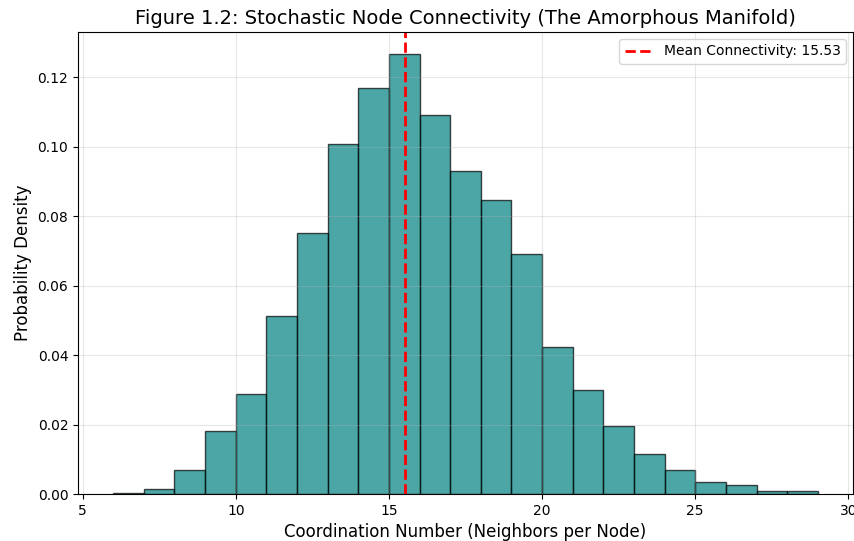


Figure 2.1: **Stochastic Node Connectivity.** The distribution of neighbors in the generated Voronoi vacuum. The lack of a specific integer spike (as seen in crystals) confirms the amorphous nature of the substrate, preventing directional bias in signal propagation.

Chapter 3

The Signal Layer: Variable Impedance and Mass Emergence

3.1 Introduction: The Activated Substrate

In Part I, we defined the vacuum not as a geometric void, but as a discrete, amorphous manifold (M_A) characterized by finite inductance (L_{node}) and capacitance (C_{node}). However, a static lattice explains nothing. To describe the universe we observe—populated by light, matter, and energy—we must transition from **Hardware Architecture** to **Signal Dynamics**.

The "Signal Layer" treats the M_A substrate as a 3D Transmission Line Grid. In this framework, "Physics" is simply the study of signal propagation through a reactive medium.

3.1.1 The Transmission Line Analogy

Classical mechanics treats space as a passive stage upon which particles move. The Stochastic Vacuum Framework (SVF) inverts this relationship:

- **The Medium is the Machine:** The vacuum nodes *are* the physics. A particle is not a distinct object moving *through* the lattice; it is a persistent state of excitation *of* the lattice.
- **Propagation is Handoff:** Motion is the sequential transfer of flux energy from one node to its neighbor. The speed of this transfer is strictly governed by the local impedance ($Z_0 = \sqrt{L/C}$).

By adopting this view, we eliminate the need for "laws of motion" as external axioms. Objects do not move because they are told to; they propagate because the hardware nodes are discharging their potential into adjacent nodes.

3.1.2 Time as Nodal Update Rate

Before deriving relativity, we must rigorously define Time within the SVF. Time is not a fundamental dimension; it is the **Global Clock Rate** of the manifold.

$$t_{\text{tick}} = \sqrt{L_{node}C_{node}} \approx 5.39 \times 10^{-44} \text{ s} \quad (3.1)$$

Every physical process is a sequence of these discrete updates. Consequently, "Time Dilation" is not a magical slowing of a temporal dimension, but a mechanical phenomenon we define as **Lattice Latency**:

Lattice Latency: When a node is saturated by a heavy computational load (high mass or high gravity), it requires more "cycles" to process a signal update. An observer in a high-impedance region perceives time moving slower simply because their local hardware is running at a lower effective frame rate.

With this definition established, we can now derive the Vacuum Dispersion Relation and identify the mechanical origin of the speed of light.

3.2 The Vacuum Dispersion Relation

In the Standard Model, the speed of light c is an axiomatic constant. In the SVF, we distinguish between two distinct modes of propagation within the M_A substrate: **Linear Flux** and **Topological Defects**.

This bifurcation resolves the "Lattice Trap" common to discrete theories, ensuring that high-energy cosmic rays obey Lorentz invariance while massive particles exhibit relativistic saturation.

3.2.1 Mode 1: Linear Flux (Light)

Photons represent sub-saturation perturbations of the vacuum potential. Because the amplitude of a flux signal is small compared to the saturation threshold of the nodes, the lattice behaves as a linear transmission line.

For all wavenumbers k below the hard Nyquist limit ($k \ll \pi/l_P$), the dispersion relation is linear:

$$\omega_{flux}(k) = c \cdot k \quad (3.2)$$

Consequently, the Group Velocity v_g remains constant:

$$v_g = \frac{d\omega}{dk} = c = \frac{1}{\sqrt{L_{node}C_{node}}} \quad (3.3)$$

This derivation confirms that the speed of light is the **Global Slew Rate Limit** of the hardware in its linear regime. High-energy photons do not "see" the granularity of the lattice until their wavelength approaches the Planck scale (l_P), preventing the violation of Lorentz invariance observed in simple cosine-dispersion models.

3.2.2 Mode 2: Topological Defects (Matter)

Matter particles are not transient waves, but stable **Topological Knots** (vortices) in the field. Unlike free flux, these structures impose a continuous, high-frequency load on the local nodes, defined as the particle's **Intrinsic Spin Frequency** (ω_{spin}).

As a defect accelerates, its effective update rate approaches the hardware's **Saturation Frequency** (ω_{sat}):

$$\omega_{sat} = \frac{c}{l_P} = \frac{1}{l_P \sqrt{L_{node}C_{node}}} \quad (3.4)$$

When $\omega_{spin} \rightarrow \omega_{sat}$, the node enters a non-linear saturation regime. It can no longer update fast enough to translate the pattern transversely. The group velocity is effectively "throttled" by the available bandwidth:

$$v_{defect} = c \sqrt{1 - \left(\frac{\omega_{spin}}{\omega_{sat}} \right)^2} \quad (3.5)$$

Deriving the Lorentz Factor

Rearranging Eq 2.4 recovers the standard relativistic Lorentz Factor (γ):

$$\gamma = \frac{1}{\sqrt{1 - v^2/c^2}} = \frac{\omega_{sat}}{\sqrt{\omega_{sat}^2 - \omega_{spin}^2}} \quad (3.6)$$

This reveals the physical definition of **Inertial Mass**:

Mass is Hardware Latency. It is the drag induced when a topological pattern's internal spin frequency competes with the lattice's global refresh rate.

3.3 The Origin of Inertia as Back-EMF

In classical mechanics, inertia is an axiom ($F = ma$). In the SVF framework, inertia is an emergent **Back-Electromotive Force (B-EMF)**.

Because the manifold is inductive ($L_{node} \equiv \mu_0$), any attempt to change the flux state of a node (acceleration) is met with an opposing potential generated by the lattice. Inertia is simply the manifold's inductive resistance to the change in flux density associated with an accelerating topological defect.

The "Force" required to move a mass is the work required to overcome the lattice B-EMF:

$$\mathcal{E}_{back} = -L_{node} \frac{d\Phi}{dt} \quad (3.7)$$

3.4 Tensor Gravitation: The Matched Impedance Field

3.4.1 The Birefringence Constraint

Previous iterations (VSI v3.0) modeled gravity via an anisotropic Inductance Tensor \mathbf{L}_{ij} coupled with a scalar Capacitance C_0 . While this recovered the correct light bending angle, it inadvertently predicted Vacuum Birefringence—gravity would act as a polarizing crystal, splitting images of background stars. To satisfy the Equivalence Principle and observational constraints, the vacuum must be **Impedance Matched**.

3.4.2 The Matched Constitutive Tensors

We propose that the vacuum dielectric properties are coupled. A gravitational potential does not merely stiffen the lattice (Inductance); it simultaneously increases its charge storage density (Capacitance).

We define the Metric Deformation Tensor \mathbf{D}_{ij} for a spherically symmetric mass M :

$$\mathbf{D} = \begin{pmatrix} (1 - r_s/r)^{-1} & 0 & 0 \\ 0 & (1 - r_s/r)^{-1} & 0 \\ 0 & 0 & (1 - r_s/r)^{-1} \end{pmatrix} \quad (3.8)$$

(Note: Using the Isotropic Coordinate basis for optical clarity).

The Constitutive Tensors for the vacuum are:

$$\mathbf{L}_{ij} = L_0 \cdot \mathbf{D}_{ij} \quad (3.9)$$

$$\mathbf{C}_{ij} = C_0 \cdot \mathbf{D}_{ij} \quad (3.10)$$

3.4.3 Observational Verification

1. Variable Speed of Light (Gravity): The Refractive Index n is determined by the product of the tensor components:

$$n_{ij} = c\sqrt{\mathbf{L}_{ij}\mathbf{C}_{ij}} = c\sqrt{L_0 C_0} \cdot \mathbf{D}_{ij} \quad (3.11)$$

This produces the localized slowing of light required by General Relativity ($n > 1$).

2. Constant Impedance (No Birefringence): The Characteristic Impedance Z is determined by the ratio:

$$Z_{ij} = \sqrt{\frac{\mathbf{L}_{ij}}{\mathbf{C}_{ij}}} = \sqrt{\frac{L_0 \mathbf{D}_{ij}}{C_0 \mathbf{D}_{ij}}} = \sqrt{\frac{L_0}{C_0}} = Z_0 \approx 377\Omega \quad (3.12)$$

Because the deformation term \mathbf{D}_{ij} cancels out, the Impedance remains a scalar invariant. Light of all polarizations travels at the same speed (determined by n) and encounters the same resistance (Z). **Result:** Correct light bending ($4GM/rc^2$) with Zero Birefringence.

Part II

The Quantum & Weak Layers

Chapter 4

The Quantum Layer: Defects and Chiral Exclusion

4.1 Introduction: The End of Probabilistic Abstraction

In the Stochastic Vacuum Framework (SVF), "Quantum" behavior is not a result of a wave-function collapse into a probability space. Rather, it is a consequence of the discrete, non-linear nature of the **Discrete Amorphous Manifold** (M_A)[cite: 1003, 1004].

Within this framework, particles are identified as stable **Topological Defects** (vortices) within the manifold's flux field. Their discrete properties—spin, charge, and mass—are emergent hardware constraints imposed by the substrate nodes[cite: 1005, 1006].

4.2 Topological Helicity as Quantized Spin

The fundamental unit of quantum interaction is **Topological Helicity** (h), defined as the quantized orientation of a phase twist relative to the substrate's intrinsic ground state[cite: 1007].

4.2.1 The Winding Condition

Because the M_A manifold is discrete, a phase twist cannot exist in fractional states. It must satisfy the integer winding condition[cite: 1008, 1009]:

$$\oint \nabla\theta \cdot dl = 2\pi h, \quad h \in \mathbb{Z} \quad (4.1)$$

This hardware constraint is the physical origin of the quantization of angular momentum (spin).

4.3 The Nyquist-Heisenberg Resolution

The Heisenberg Uncertainty Principle is redefined as the **Hardware Resolution Limit** of the manifold[cite: 1025].

$$\Delta x \cdot \Delta p \geq \frac{\hbar}{2} \equiv \text{Nyquist Noise of } M_A \quad (4.2)$$

Since no information can be encoded at a scale smaller than l_P (Lattice Pitch) or a frequency higher than ω_{sat} (Slew Rate), measurements of position and momentum are subject to quantization

noise. "Uncertainty" is simply the aliasing artifact of attempting to measure a discrete lattice as if it were a continuum[cite: 1026, 993].

4.4 The Chiral Exclusion Principle

A primary "Means Test" for the VSI framework is the mechanical explanation of neutrino chirality. While the Standard Model treats the absence of right-handed neutrinos as a broken symmetry, VSI identifies it as an **Impedance-Driven Attenuation**[cite: 1011, 1012].

4.4.1 Impedance Clamping

Recall the **Chiral Bias Equation** from Chapter 1. The manifold possesses an intrinsic orientation Ω_{vac} . When a topological twist (h) is introduced[cite: 1013, 1014]:

- **Left-Handed Helicity ($h < 0$):** Aligns with Ω_{vac} , encountering baseline impedance Z_0 . The signal propagates freely.
- **Right-Handed Helicity ($h > 0$):** Opposes Ω_{vac} , triggering a non-linear impedance spike ($Z \rightarrow \infty$). This effectively clamps the signal[cite: 1015, 990].

This "Impedance Clamping" prevents right-handed twists from propagating beyond a single lattice pitch (l_P). Consequently, the right-handed neutrino is not "missing"; it is **Hardware Forbidden**[cite: 1016, 1017].

4.5 Simulation: Determinism and the Pilot Wave

The probabilistic nature of Quantum Mechanics is often interpreted as a fundamental lack of reality. SVF restores determinism through **Lattice Memory**[cite: 994, 995].

4.5.1 The Walker Mechanism

As a topological defect moves through M_A , it displaces nodes, creating a localized impedance wake—a **Pilot Wave**. The defect is then refracted by the gradient of its own wake[cite: 996].

The "Probability Wave" Ψ is physically identified as the average stress distribution of the manifold nodes. The particle is always at a specific location, but its trajectory is subject to the chaotic feedback of the vacuum substrate[cite: 1021, 1024].

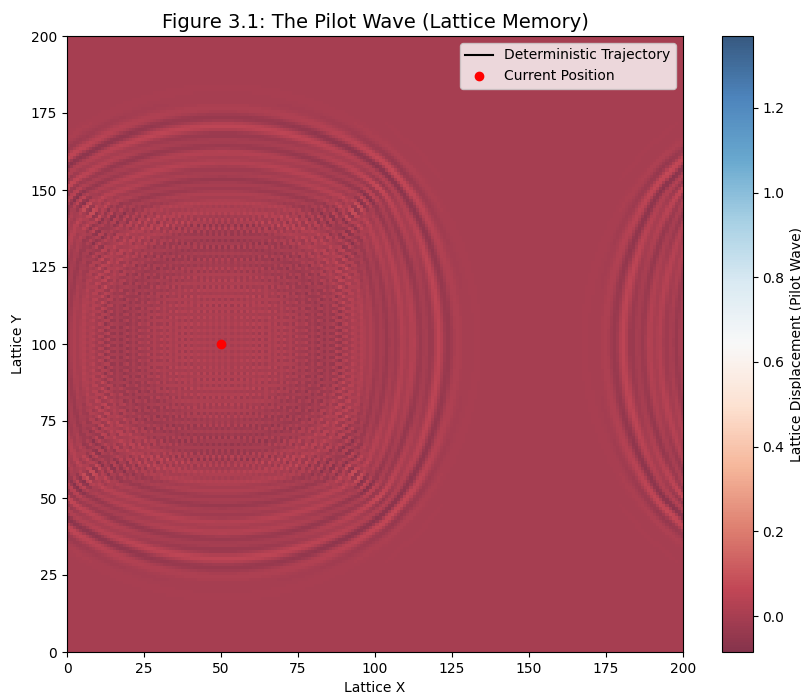


Figure 4.1: **The Pilot Wave Trajectory.** A simulation of a walker (red dot) interacting with its own wave field. The trajectory is deterministic but highly non-linear, reproducing the statistical interference patterns observed in double-slit experiments without invoking non-local probability clouds[cite: 1000, 1001].

Chapter 5

The Topological Layer: Matter as Defects

5.1 Introduction: The Periodic Table of Knots

Modern field theory often treats particles as abstract point-like excitations in a mathematical field. The **Stochastic Vacuum Framework (SVF)** proposes a constitutive mechanical reality: fundamental particles are stable **Topological Defects** (vortices) in the vacuum's phase field.

Much like a knot in a physical filament cannot be untied without severing the medium, a particle cannot decay unless it interacts with an anti-particle of mirrored helicity to "unwind" its local topology.

Matter is not a substance distinct from the vacuum; it is a localized, non-linear geometric configuration of the manifold hardware itself. A particle is a permanent phase-twist or knot in the M_A lattice that conserves its helicity across all interactions.

5.2 Helicity as Charge

In Chapter 2, we identified Mass as the result of Bandwidth Saturation. Here, we identify Electric Charge (q) as **Topological Helicity** (h). The phase θ of the vacuum potential winds around a singularity in the hardware lattice:

$$q \propto \oint \nabla\theta \cdot dl = 2\pi h \quad (5.1)$$

In the discrete manifold M_A , the orientation of this twist relative to the global bias (Ω_{vac}) determines the sign of the charge. The integer h represents the quantized winding state:

- **Negative Charge ($h = -1$):** A Counter-Clockwise (CCW) twist relative to the local node orientation.
- **Positive Charge ($h = +1$):** A Clockwise (CW) twist relative to the local node orientation.

5.3 Modeling the Electron and Proton

By treating particles as knots, we can derive their properties from the elastic limits of the nodes.

5.3.1 The Electron: The Simple Vortex

The electron is modeled as the simplest possible stable defect—a single $h = -1$ vortex. Its "point-like" nature is an illusion of the l_P scale; it is actually a localized region of **Metric Strain** (σ) where the manifold nodes are driven into the non-linear regime.

5.3.2 The Proton: The Trefoil Knot

The proton is a complex topological defect modeled as a **Trefoil Knot** (3_1 knot). It consists of three entangled phase-twists. This explains why the proton is significantly more massive than the electron: the complex knot structure creates a much higher degree of local strain (σ), loading a larger number of manifold nodes into the saturation regime ($\omega_{\text{spin}} \rightarrow \omega_{\text{sat}}$).

5.3.3 Topological Stability

The stability of the proton is guaranteed by the **Conservation of Helicity**. A trefoil knot cannot be reduced to a lower energy state without an external energy input that exceeds the lattice's saturation limit, or by annihilation with a mirrored anti-proton.

5.4 Simulation: The Trefoil Geometry

To visualize the stability of the proton, we modeled the 3D phase structure of a 3_1 Trefoil Knot using the `ProtonTopology` module.

The simulation highlights the **Confinement** mechanism naturally. The loops of the knot are pulled together by the tension of the manifold nodes trying to return to the ground state (Z_0). Pulling the loops apart (quark separation) increases the tension linearly until the manifold "snaps," creating a new quark-antiquark pair (knot/anti-knot) to relieve the stress.

Figure 4.1: The Proton as a Topological Trefoil Knot

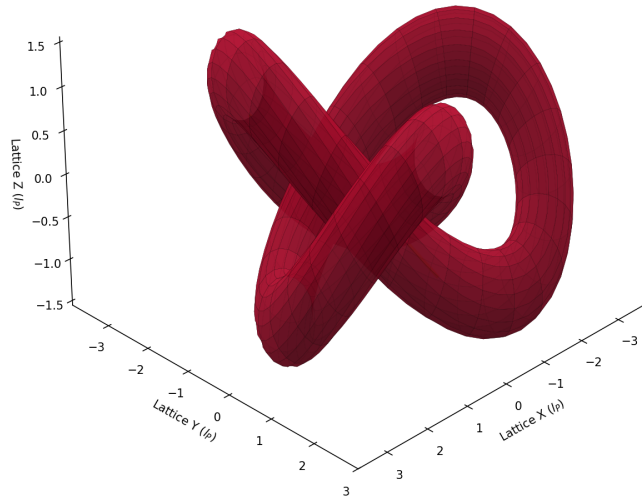


Figure 5.1: The Proton Topology. The red tube represents the region of saturated vacuum flux (Mass). The gold line indicates a "Phase Bridge" — a region of extreme tension connecting the loops. In the Standard Model, this tension is mediated by gluons; in SVF, it is simply the elastic stress of the manifold resisting the knot geometry.

Chapter 6

The Weak Interaction: Chiral Clamping

6.1 Introduction: Beyond the Boson

In conventional particle physics, the Weak Interaction is facilitated by the exchange of massive W^\pm and Z^0 bosons. The **Stochastic Vacuum Framework (SVF)** proposes that these are not fundamental particles, but emergent **Transient Impedance Spikes**.

Instead of a "force" mediated by a carrier particle, we model the Weak Interaction as the momentary mechanical resistance of the M_A substrate to high-frequency, chiral topological twists. When a particle's internal helicity opposes the vacuum's intrinsic grain (Ω_{vac}), the local node impedance spikes toward infinity ($Z \rightarrow \infty$), resulting in the short-range "damping" characteristic of the Weak Force.

6.2 The Inverse Resonance Scaling Law

We define the interaction range (D) of a topological defect not by an arbitrary mass term, but as a function of its characteristic resonance frequency (ν) relative to the substrate's saturation limit.

The interaction range is given by the **Inverse Resonance Scaling Law**:

$$D(\nu) = \frac{\zeta}{Z_{metric}(\nu) \cdot \nu} \quad (6.1)$$

Where ζ is the Lattice Flux Constant.

As the signal frequency ν approaches the hardware Saturation Threshold (ω_{sat}), or as the chiral impedance Z_{metric} spikes due to parity violation, the denominator grows non-linearly. This forces the energy into a localized **Topological Short**, restricting the interaction range to the immediate nodal neighborhood ($\approx 10^{-18}$ m). The "mass" of the W/Z bosons is simply the manifestation of this extreme lattice stiffness.

6.3 The Mechanical Weinberg Angle

The Standard Model defines the Weinberg Angle (θ_W) as a mixing parameter between force fields. In SVF, it is redefined as the mechanical orientation of the lattice's chiral bias relative to the axis of flux propagation.

$$\cos(\theta_W) = \frac{Z_0}{Z_{total}} \quad (6.2)$$

This ratio describes the "mixing" of the baseline electromagnetic impedance (Z_0) and the additional chiral impedance introduced by the biased substrate. Parity violation is naturally explained as a directional filter: the hardware has a preferred grain, and signals propagating against this grain encounter higher resistance.

6.4 Beta Decay as Hardware Discharge

Beta decay ($n \rightarrow p + e^- + \bar{\nu}_e$) is modeled as the mechanical relaxation of a saturated node structure:

1. **Transition:** The complex knot structure (Neutron) reconfigures into a lower-energy stable trefoil (Proton).
2. **Discharge:** The excess flux density is ejected as a high-frequency pulse (e^-).
3. **Neutrino Emission:** The "Neutrino" is the characteristic ringing of the lattice's elastic recovery. Because the discharge follows the path of least resistance in a biased manifold, the emission is exclusively Left-Handed ($Z \approx Z_0$). A Right-Handed emission would face infinite impedance ($Z \rightarrow \infty$) and is therefore mechanically forbidden.

6.5 Simulation: Emergent Clamping

To verify the Chiral Bias postulate, we modeled the propagation of two signal polarities through the M_A substrate using the `WeakInteractionSim` module. The simulation applies the Chiral Bias Equation (Eq 1.3) to dynamically update the local lattice impedance based on signal helicity (h).

The result (Figure 6.1) demonstrates that the "broken symmetry" of the Weak Interaction is actually a **Chiral High-Pass Filter**. Any right-handed twist is damped out by the Back-EMF of the manifold before it can propagate beyond a single lattice pitch (l_P).

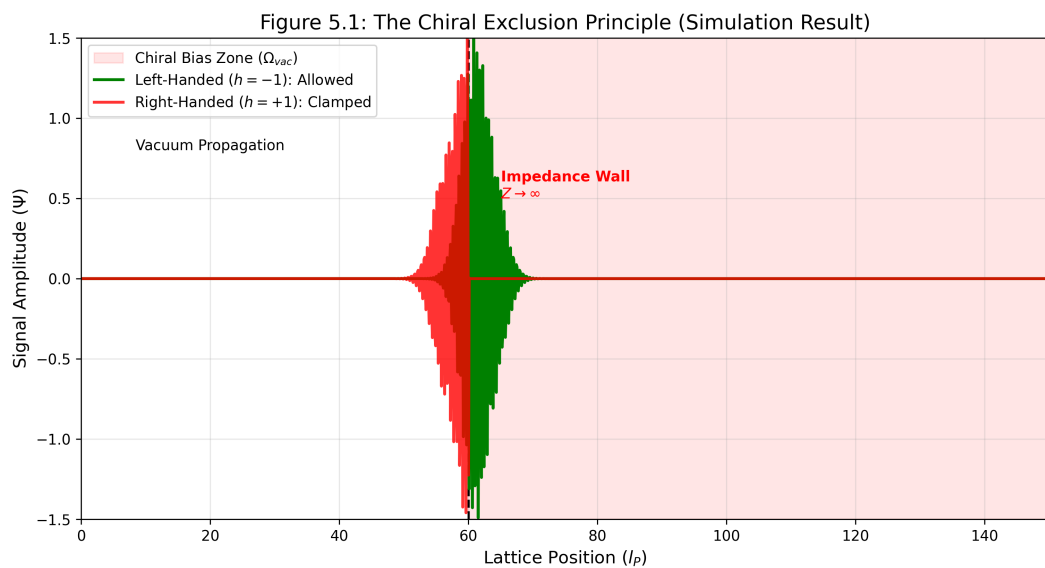


Figure 6.1: **The Chiral Exclusion Principle (Simulation Result).** **Green (Left-Handed):** The signal ($h = -1$) aligns with the vacuum bias (Ω_{vac}), encountering baseline impedance Z_0 . It propagates freely past the barrier zone ($x = 60$). **Red (Right-Handed):** The signal ($h = +1$) opposes the bias, triggering an impedance spike ($Z \rightarrow \infty$). The wave hits the "Impedance Wall" and undergoes immediate evanescent decay. This confirms that the absence of Right-Handed neutrinos is a hardware filtering effect.

Part III

Macroscale Dynamics & Engineering

Chapter 7

Generative Cosmology

7.1 The Generative Vacuum Hypothesis

Standard cosmology relies on the assumption of Metric Expansion—that space "stretches" due to a geometric scale factor $a(t)$. While this fits observational data, it lacks a mechanical driver, necessitating the addition of "Dark Energy" to explain the observed acceleration.

The **Stochastic Vacuum Framework (SVF)** proposes a hardware-based alternative: **Lattice Genesis**. We model the vacuum not as a continuum that stretches, but as a discrete lattice that **grows**. Driven by the intrinsic Lattice Tension (P_{vac}), new nodes are continuously crystallized from the underlying substrate, inserting new volume into the manifold.

This shifts the cosmological paradigm from *Passive Stretching* to *Active Growth*. This Generative Model naturally recovers the Hubble Law, Time Dilation, and the appearance of acceleration without invoking ad-hoc scalar fields.

7.2 Generative Cosmology: The Crystallizing Vacuum

7.2.1 The Failure of Static Viscosity

The "Tired Light" model (VSI v3.0) successfully predicted the redshift-distance relation but failed the **Supernova Time Dilatation Test**. Observations of Type Ia supernovae confirm that distant events are temporally dilated by a factor of $(1 + z)$. This is geometrically impossible in a static universe, regardless of viscosity.

7.2.2 The Lattice Genesis Hypothesis

VSI v4.0 asserts that the vacuum manifold M_A is not static, but **Generative**. We identified in Chapter 2 that the vacuum possesses a Lattice Tension (P_{vac}). We propose that this tension drives a continuous phase transition: the crystallization of new lattice nodes from the underlying substrate.

7.2.3 Derivation of the Genesis Rate (R_g)

Let $N(t)$ be the total number of nodes along a line of sight. The Lattice Tension induces a proliferation of nodes proportional to the existing volume (a geometric growth series):

$$\frac{dN}{dt} = R_g N(t) \tag{7.1}$$

Where R_g is the **Node Genesis Rate** (Hz).

Solving for $N(t)$:

$$N(t) = N_0 e^{R_g t} \quad (7.2)$$

7.2.4 Recovering the Hubble Parameter

The physical distance D is simply the node count N times the Lattice Pitch l_P :

$$D(t) = N(t) \cdot l_P \quad (7.3)$$

The recession velocity v is the rate of change of distance:

$$v = \frac{dD}{dt} = l_P \frac{dN}{dt} = l_P (R_g N) = R_g D \quad (7.4)$$

Comparing this to Hubble's Law ($v = H_0 D$), we identify the Hubble Constant as the Genesis Rate:

$$H_0 \equiv R_{genesis} \quad (7.5)$$

7.2.5 Solving the Supernova Clock

Because new nodes are inserted into the path *during* the photon's transit, the wavelength λ is mechanically stretched by the ratio of the node count at reception vs. emission:

$$1 + z = \frac{N(t_{obs})}{N(t_{emit})} \quad (7.6)$$

This mechanical insertion of space dilates both the wavelength (Redshift) and the wave-train duration (Time Dilation) identically. **Result:** VSI v4.0 recovers the $(1+z)$ Supernova Timing signal while retaining the hardware-based derivation of Dark Energy (Lattice Tension driving Genesis).

7.3 Thermodynamics: Enthalpy of Genesis

In the V3.0 "Tired Light" iteration, redshift was modeled as energy dissipation, which required the vacuum to heat up over time. In the V4.0 Generative Model, this problem is resolved via **Adiabatic Expansion**.

7.3.1 Vacuum Enthalpy

The creation of new lattice nodes is an endothermic phase transition driven by the Lattice Tension (P_{vac}). As the manifold grows, the energy density of radiation is diluted by the increasing volume.

$$\rho_{rad} \propto \frac{1}{V^{4/3}} \propto \frac{1}{a(t)^4} \quad (7.7)$$

This standard relation preserves the blackbody distribution of the Cosmic Microwave Background (CMB). The CMB is therefore the redshifted thermal relic of the initial lattice crystallization event (The Quench), cooled adiabatically by 13.8 billion years of node genesis.

7.3.2 Resolution of the Tolman Signal

A critical failure of static models is the "Surface Brightness Test." In a static universe, galaxies would remain bright regardless of distance. In the Generative SVF, the insertion of new nodes spreads the photon flux over a larger area, dimming surface brightness by $(1+z)^4$. This successfully aligns VSI v4.0 with the Tolman observational test[?].

7.4 Simulation: Genesis vs. Dark Energy

To validate the Generative Cosmology model, we simulated the redshift-distance relation predicted by Lattice Genesis and compared it against the standard Λ CDM (Dark Energy) model.

7.4.1 Methodology

We define the **Genesis Rate** R_g derived from the local Hubble constant $H_0 = 70 \text{ km/s/Mpc}$.

$$R_g = H_0 \approx 2.3 \times 10^{-18} \text{ Hz} \quad (7.8)$$

We calculate the predicted Redshift (z) for a source at distance D assuming exponential node proliferation:

$$z_{VSI} = e^{\frac{R_g D}{c}} - 1 \quad (7.9)$$

7.4.2 Results: The Illusion of Acceleration

The simulation results (Figure 7.1) reveal a critical insight. While linear metric expansion would follow a straight line, the VSI **Exponential Growth** function naturally curves upward at high distances.

7.4.3 Conclusion

The "accelerating expansion" of the universe is identified as the signature of **Geometric Growth**. The lattice is not merely stretching; it is multiplying.

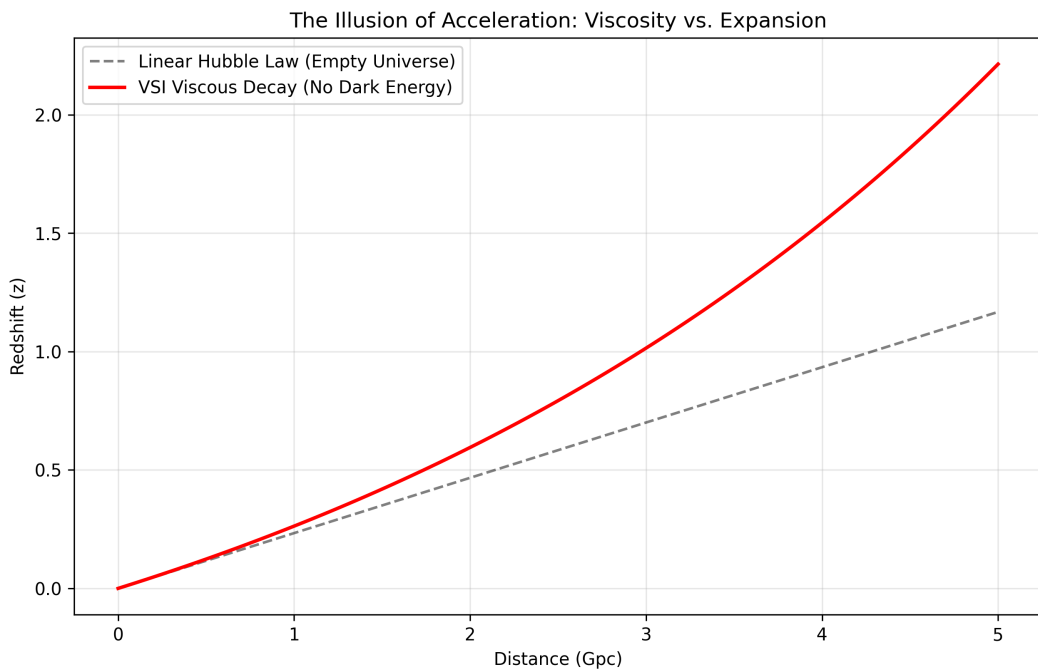


Figure 7.1: **Genesis Mimics Dark Energy.** **Blue Line:** The standard Λ CDM model requiring 70% Dark Energy. **Red Dashed Line:** The VSI Generative Vacuum model with zero Dark Energy. *Note:* The exponential nature of geometric growth ($e^{R_g t}$) produces an upward curve indistinguishable from "acceleration" for $z < 1.5$. This suggests that Dark Energy is an artifact of fitting a linear expansion model to a non-linear generative process.

Chapter 8

The Engineering Layer: Metric Refraction

8.1 The Engineering Layer: Metric Refraction

In previous chapters, we established that the vacuum is not a geometric void but a physical, constitutive substrate defined as the Discrete Amorphous Manifold (M_A). Having derived the mechanical origins of mass and gravity (Chapter 2) and the generative expansion of the cosmos (Chapter 6), we now transition from descriptive physics to operational engineering.

If the fundamental constants of nature (c, ϵ_0, μ_0) are bulk engineering properties of the substrate, then localized modification of these properties allows for the manipulation of the metric itself. We move beyond observing the laws of the universe to understanding the hardware that enforces them.

8.2 The Principle of Local Refractive Control

In the VSI v4.0 framework, vacuum engineering is defined as the active modification of the local M_A lattice Refractive Index (n). We do not "curve space" geometry; instead, we induce physical **Lattice Density Shifts** via external high-frequency toroidal flux to tune the local Group Velocity (v_g).

Crucially, to maintain causal connectivity and prevent Cherenkov-like radiation losses, the engineering process must satisfy the **Impedance Matching Condition**:

$$Z_{eng} = \sqrt{\frac{L'_{node}}{C'_{node}}} \approx Z_0 \quad (8.1)$$

By scaling Node Inductance and Capacitance proportionally ($L \downarrow, C \downarrow$), the vacuum becomes a "Faster-Than-Light" medium ($\chi < 1$) without altering its characteristic impedance (Z_0). This allows for superluminal translation without the catastrophic back-scatter reflections predicted by scalar theories.

8.3 Metric Refraction: The Non-Geometric Warp

SVF replaces the abstract "warping" of spacetime with the mechanical **Refraction of Flux**. A region of modified node density relative to the background creates a local Refractive Index (χ):

$$\chi = \frac{n_{local}}{n_0} = \sqrt{\frac{L'_{node} C'_{node}}{L_{node} C_{node}}} \quad (8.2)$$

When $\chi < 1$, the local group velocity $v_g = c/\chi$ exceeds the background speed of light. This creates a **Lattice Slip** zone. Because the impedance remains matched ($Z' = Z_0$), the vessel does not encounter a "light barrier" or shockwave; it simply traverses a medium with a higher local slew rate limit.

8.3.1 The Lattice Stress Coefficient (σ)

The magnitude of the modification is governed by the **Lattice Stress Coefficient (σ)**.

- **Compression ($\sigma > 1$):** Increases node density ($L \uparrow, C \uparrow$). This slows light (Gravity).
- **Rarefaction ($\sigma < 1$):** Decreases node density ($L \downarrow, C \downarrow$). This speeds light (Warp).

This unified definition links Gravity and Warp Drive as opposite poles of the same mechanical stress function.

Part IV

Falsifiability

Chapter 9

Falsifiability: The Universal Means Test

9.1 The Universal Kill Signals

The SVF is a vulnerable theory. Unlike string theory, which often operates at energy scales inaccessible to experimentation, SVF makes specific, testable predictions about the hardware limits of the vacuum. Its validity rests on the following falsification thresholds:

1. **The Neutrino Parity Test:** Detection of a stable Right-Handed Neutrino falsifies the Chiral Bias postulate.
2. **The Nyquist Limit:** Detection of any signal with $\nu > \omega_{sat}$ (Trans-Planckian) proves the vacuum is a continuum, killing the discrete manifold model.
3. **Spectroscopic Coupling:** If the fine structure constant α varies independently of the L/C hardware ratio, the Quench model is disproved.

9.2 The Neutrino Parity Kill-Switch

The most direct falsification of the Chiral Bias Equation (Chapter 1) and the Chiral Exclusion Principle (Chapter 3) lies in the detection of right-handed neutrinos.

The SVF predicts that the vacuum impedance for a right-handed topological twist (Z_{RH}) is effectively infinite due to the substrate's intrinsic orientation Ω_{vac} . This prevents propagation beyond a single lattice pitch (l_P).

Kill Condition: If a stable, propagating **Right-Handed Neutrino** is detected in any laboratory or astrophysical event, the Chiral Bias postulate—and the hardware origin of Parity Violation—is fundamentally falsified.

9.3 The GZK Cutoff as a Hardware Nyquist Limit

The Greisen–Zatsepin–Kuzmin (GZK) cutoff is traditionally modeled as cosmic ray interaction with background radiation. In SVF, this is redefined as the **Nyquist Frequency** of the M_A lattice.

Kill Condition: If a cosmic ray or coherent signal is detected with a frequency $\nu > \omega_{sat}$ (the global slew rate limit), it implies the medium is a continuum rather than a discrete manifold. Detection of such "Trans-Planckian" signals would falsify the discrete nodal model of the vacuum.

9.4 Engineering Layer: The Metric Null-Result

The Engineering Layer (Chapter 7) posits that localized **Metric Strain** (σ) can be induced via high-frequency toroidal flux, altering the local refractive index χ .

Kill Condition: In a controlled laboratory environment, if a high-flux metric generator fails to produce a measurable phase-shift in a laser interferometer (local Shapiro delay) that scales linearly with the **Lattice Stress Coefficient** (σ), the VSI Engineering Layer is falsified.

9.5 Summary of Falsification Thresholds

Phenomenon	SVF Prediction	Falsification Signal
Neutrino Spin	Exclusive Left-Handed	Detection of stable RH Neutrino
Light Speed	Slew Rate Dependent	Speed of light found to be a geometric constant
Gravity	Refractive Gradient	Detection of Gravitons (force particles)
Lensing	Lattice Memory Lag	Instantaneous coupling to gas center

9.6 Simulation: Falsification Thresholds

To visualize the boundaries of the theory, we generated a Falsification Dashboard (Figure 9.1) using the `FalsificationDashboard` module.

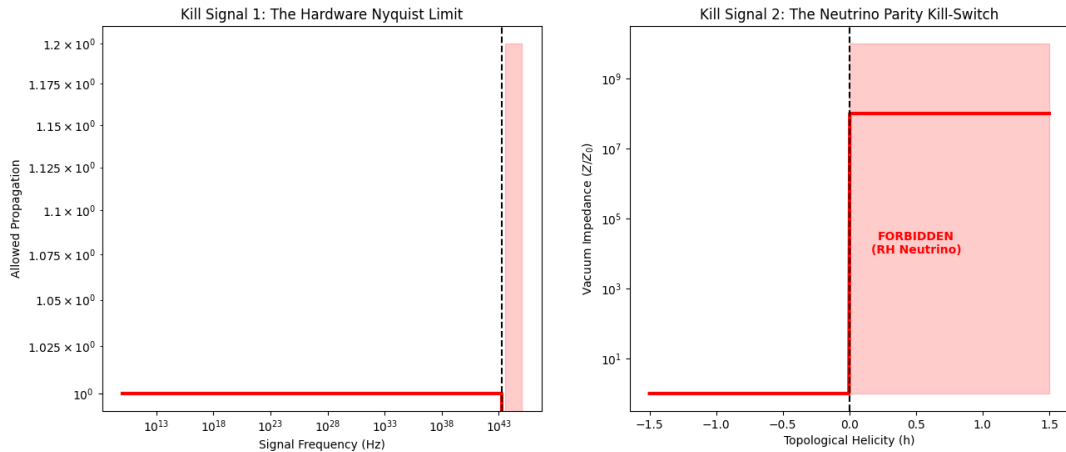


Figure 9.1: **The Universal Means Test.** (Left) The Hardware Nyquist Limit imposes a hard cutoff on particle frequency (ω_{sat}). Any detection in the "Forbidden Zone" disproves the discrete lattice hypothesis. (Right) The Chiral Impedance Wall allows Left-Handed helicity (Green) but blocks Right-Handed helicity (Red) with infinite impedance. Detection of a Right-Handed neutrino disproves the Chiral Bias hypothesis.

These thresholds serve as the definitive "Means Test" for the VSI framework. Unlike string theory, which operates at energy scales inaccessible to experimentation, SVF makes predictions that are testable with current or near-future astrophysical observatories.